

REPORT

Structural basis for the antagonistic roles of RNP-8 and GLD-3 in GLD-2 poly(A)-polymerase activity

KATHARINA NAKEL,¹ FABIEN BONNEAU,¹ CLAIRE BASQUIN,¹ BIANCA HABERMANN,¹ CHRISTIAN R. ECKMANN,² and ELENA CONTI¹

¹Department of Structural Cell Biology, Max-Planck-Institute of Biochemistry, D-82152 Martinsried, Germany

²Department of Genetics, Martin-Luther-University of Halle-Wittenberg, Institute of Biology, 06120 Halle (Saale), Germany

ABSTRACT

Cytoplasmic polyadenylation drives the translational activation of specific mRNAs in early metazoan development and is performed by distinct complexes that share the same catalytic poly(A)-polymerase subunit, GLD-2. The activity and specificity of GLD-2 depend on its binding partners. In *Caenorhabditis elegans*, GLD-2 promotes spermatogenesis when bound to GLD-3 and oogenesis when bound to RNP-8. GLD-3 and RNP-8 antagonize each other and compete for GLD-2 binding. Following up on our previous mechanistic studies of GLD-2–GLD-3, we report here the 2.5 Å resolution structure and biochemical characterization of a GLD-2–RNP-8 core complex. In the structure, RNP-8 embraces the poly(A)-polymerase, docking onto several conserved hydrophobic hotspots present on the GLD-2 surface. RNP-8 stabilizes GLD-2 and indirectly stimulates polyadenylation. RNP-8 has a different amino-acid sequence and structure as compared to GLD-3. Yet, it binds the same surfaces of GLD-2 by forming alternative interactions, rationalizing the remarkable versatility of GLD-2 complexes.

Keywords: translational regulation; cytoplasmic polyadenylation; nucleotidyl-transferase; germline development; *C. elegans*

INTRODUCTION

The poly(A) tail is a key post-transcriptional modification that impacts on the stability, export and translational efficiency of the vast majority of eukaryotic mRNAs (for review, see Moore and Proudfoot 2009 and Eckmann et al. 2011). The shortening of the poly(A) tail by cytoplasmic deadenylases is linked to translational repression and generally to the decay of the deadenylated mRNA. In germ cells and neuronal synapses in particular, deadenylation also serves to store the transcripts in a dormant state until translation is resumed upon the extension of the poly(A) tail by cytoplasmic poly(A)-polymerases (for review, see Weill et al. 2012 and Norbury 2013).

GLD-2 (germline development defective 2) is a highly conserved cytoplasmic poly(A)-polymerase in metazoans. It was discovered in *Caenorhabditis elegans* for its role in meiotic entry (Wang et al. 2002) and has since been identified and studied in other species, including *X. laevis*, *D. melanogaster*, and *M. musculus* (Barnard et al. 2004; Kwak et al. 2004; Rouhana and Wickens 2007; Benoit et al. 2008; Sartain et al. 2011). GLD-2 orthologs control many aspects of germline development, including the production of male and female gametes

(Kadyk and Kimble 1998; Eckmann et al. 2004; Hansen et al. 2004; Kim et al. 2009, 2010; Sartain et al. 2011; Cui et al. 2013; Nousch et al. 2014). In addition, they are involved in the formation of long-term memory in the brain (Kwak et al. 2008; Udagawa et al. 2012).

GLD-2 is a member of the noncanonical family of poly(A)-polymerases (Martin and Keller 2007; Schmidt and Norbury 2010). It lacks the RNA recognition motif (RRM) fold characteristic of the canonical nuclear poly(A)-polymerase and associates with a variety of binding partners that in general activate and target it to specific transcripts (Wang et al. 2002; Barnard et al. 2004; Eckmann et al. 2004; Suh et al. 2006; Papin et al. 2008; Kim et al. 2009, 2010; Cragle and MacNicol 2014). *Caenorhabditis elegans* GLD-3 is arguably the best studied GLD-2–binding partner (Eckmann et al. 2002). GLD-3 contains four noncanonical KH domains (Nakel et al. 2010). It also contains an N-terminal region that wraps around GLD-2 and increases the RNA-binding properties and the stability of the poly(A)-polymerase, thereby promoting polyadenylation (Nakel et al. 2015).

Functionally, the GLD-2–GLD-3 complex controls the transition from mitosis to meiosis (Wang et al. 2002; Crittenden et al. 2003; Eckmann et al. 2004) and spermatogenesis (Eckmann et al. 2002, 2004; Kim et al. 2009). While GLD-3

Corresponding author: conti@biochem.mpg.de

Article published online ahead of print. Article and publication date are at <http://www.rnajournal.org/cgi/doi/10.1261/rna.056598.116>. Freely available online through the RNA Open Access option.

© 2016 Nakel et al. This article, published in RNA, is available under a Creative Commons License (Attribution 4.0 International), as described at <http://creativecommons.org/licenses/by/4.0/>.

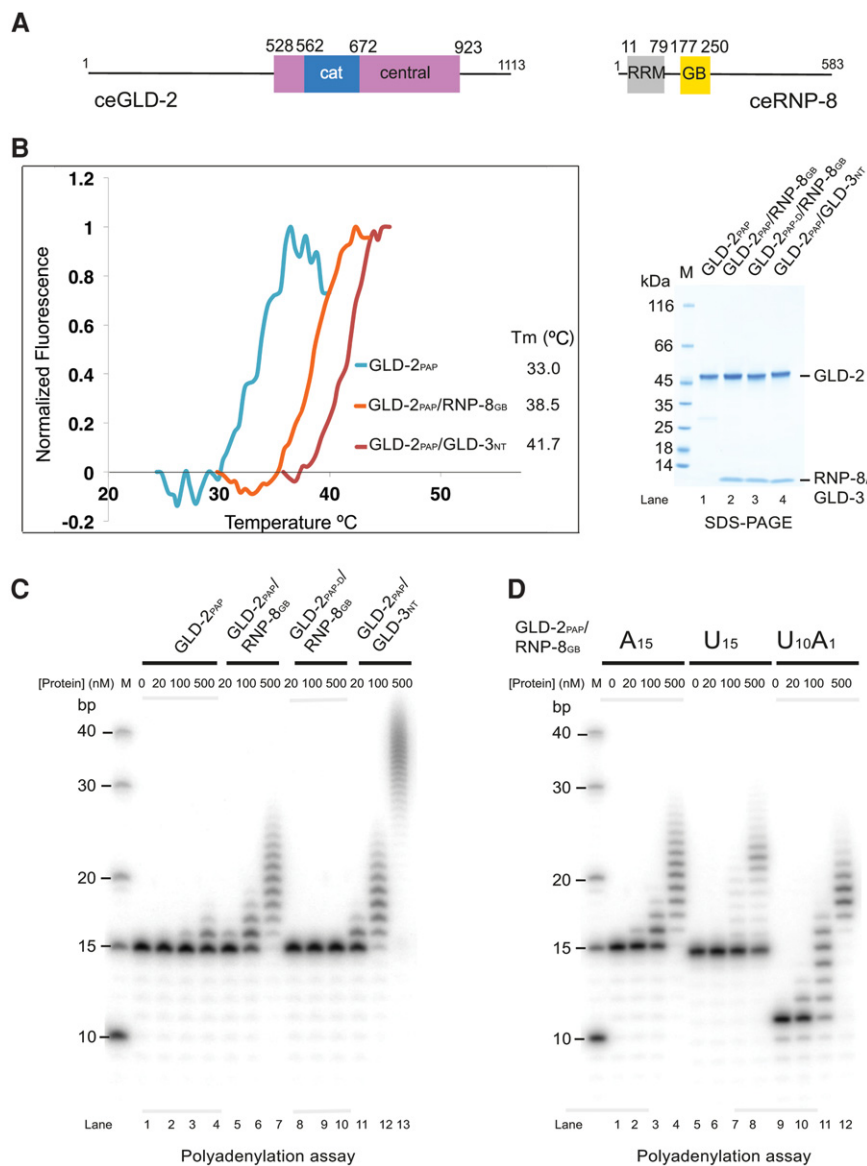


FIGURE 1. Activity of a minimal GLD-2-RNP-8 complex. (A) Schematic representation of the domain structure of *C. elegans* GLD-2 and RNP-8. Globular domains are shown as rectangles and low-complexity sequences as lines. The catalytic (cat) and central domains of GLD-2 are colored in blue and pink, respectively. As in other nucleotidyltransferases, the central domain is composed of two noncontiguous polypeptide segments, which correspond in the structure to helix $\alpha 1$ and helices $\alpha 4$ - $\alpha 8$ for the segments preceding and following the catalytic domain, respectively (see also Fig. 2). The RNA recognition motif (RRM) and the GLD-2-binding (GB) domains of RNP-8 are colored in gray and yellow, respectively. (B) Protein stability of GLD-2_{PAP}-RNP-8_{GB}, GLD-2_{PAP}-GLD-3_{NT}, and GLD-2_{PAP} as determined by thermofluor experiments. The normalized curves and the corresponding melting temperatures are shown on the left. The Coomassie-stained 4%–15% Bio-Rad TGX SDS-PAGE gel of the proteins used in the thermofluor and poly(A) polymerase assays (C,D) are shown on the right and in Supplemental Figure 1C. (C) Polyadenylation assay of *C. elegans* GLD-2_{PAP} or GLD-2_{PAP-D} in complex with either RNP-8_{GB} or GLD-3_{NT} (Nakel et al. 2015). (D) Polyadenylation assay of GLD-2_{PAP}-RNP-8_{GB} (0, 20, 100, and 500 nM) in the presence of 5'-³²P-labeled A₁₅, U₁₅, or U₁₀A₁ oligomers (100 nM).

favors sperm fate, another GLD-2 binding protein, RNP-8, favors oocyte fate (Kim et al. 2009, 2010). RNP-8 and GLD-3 genetically antagonize each other for gamete production and form separate complexes with GLD-2 in vitro and in vivo

(Kim et al. 2009, 2010). However, RNP-8 does not share apparent sequence similarity with GLD-3, raising the question of how the two proteins can compete for GLD-2 binding and activation. In this work, we used biochemical and structural studies to obtain insights into the molecular mechanisms.

RESULTS AND DISCUSSION

We previously characterized a nucleotidyl-transferase region of *C. elegans* GLD-2 suitable for biochemical and structural studies with the corresponding binding domain of GLD-3 (Nakel et al. 2015). We will refer to these fragments as GLD-2_{PAP} for the wild-type enzyme, and GLD-2_{PAP-D} for the catalytically dead D668A mutant (Fig. 1A; Materials and Methods). For GLD-3, we will refer to the N-terminal GLD-2 binding domain as GLD-3_{NT} (residues 13–88). Yeast-two-hybrid assays have identified a 39-residue segment in the unstructured C-terminal region of RNP-8 (residues 186–224) as the GLD-2 interaction site (Kim et al. 2009). We coexpressed GLD-2_{PAP} with a slightly larger RNP-8 fragment (residues 171–250), and found it proteolyzed spontaneously to residues 177–250 (referred to as RNP-8_{GB} for GLD-2 binding) (Fig. 1A; Supplemental Fig. 1A,B). GLD-2_{PAP} and RNP-8_{GB} co-purified in a binary complex with increased stability as compared to GLD-2_{PAP} in isolation (Fig. 1B; Supplemental Fig. 1C). GLD-2_{PAP}-RNP-8_{GB} had poly(A)-polymerase activity in vitro on an A₁₅ RNA substrate, albeit less robust than for GLD-2_{PAP}-GLD-3_{NT} (Fig. 1C). Finally, GLD-2_{PAP}-RNP-8_{GB} showed a preference for an RNA substrate with adenosines at the 3' end (Fig. 1D), similarly to GLD-2_{PAP}-GLD-3_{NT} (Nakel et al. 2015).

We determined the structure of GLD-2_{PAP-D}-RNP-8_{GB} at a resolution of 2.5 Å and R_{free} of 24.2% (Table 1). The four independent copies of the complex in the asymmetric unit are very similar (with the exception that only two have the active site occupied by a magnesium ion and a peptide originating from a crystal-packing interaction, Supplemental Fig. 1D). In the text, we describe one of the complexes (chains A and E) unless otherwise specified. The final model includes

residues 544–922 of GLD-2 (with the exception of missing or disordered residues between 815–860 and 879–882) and residues 177–222 of RNP-8. The overall structure of GLD-2_{PAP-D} has the typical features of nucleotidyl-transferases (for review, see Martin and Keller 2007). Briefly, the catalytic and central domains face each other forming a V-shaped cleft in between (Fig. 2A). Based on the substrate-bound structure of canonical PAP (Balbo and Bohm 2007) the cleft in GLD-2 is expected to contain the binding sites for RNA and ATP as well as the catalytic residues.

There are two major differences of GLD-2 in the RNP-8_{GB} structure as compared to the previous GLD-3_{NT} structure (Nakel et al. 2015). First, the catalytic domain is rotated toward the central domain and has a closer conformation of the active-site cleft (Fig. 2A). Second, the top of the central domain forms more rigid secondary structure elements, with a well-defined four-stranded β -sheet (β_6 – β_9) lining the entrance of the cleft (Fig. 2A). In other nucleotidyl-transferases, this part of the molecule contains elements that determine the nucleotide specificity (the so-called nucleotide recognition motif or NRM [Schmidt and Norbury 2010]). Both differences are likely related to a crystallization effect: The active-site cleft binds the N-terminal residues of the RNP-8_{GB} polypeptide of a neighboring molecule in the lattice. With hindsight, residues 177–182 of RNP-8_{GB} mimic binding of RNA and ATP and appear essential for crystallization. This substrate mimic is remarkable (Fig. 2B), suggesting that GLD-2 was serendipitously crystallized in an active-like conformation.

RNP-8_{GB} wraps around GLD-2_{PAP-D}, burying more than 1800 Å² (35%) of its accessible surface area as calculated with PISA (Krissinel and Henrick 2007), with extensive interactions distributed over three distinct patches (Figs. 2A, 3A,B). In the N-terminal half of RNP-8_{GB}, residues 183–198 adopt an extended conformation as they stretch around the helical side of the catalytic domain (patch 1). RNP-8 Pro183, Phe190, Ile193, Phe195, and Phe197 interact with exposed hydrophobic residues of GLD-2 (Fig. 3B, left panel). RNP-8_{GB} then continues with a five-turn helix that wedges in between the catalytic

and central domain (patch 2, Fig. 3B, middle panel). On one side of the helix, RNP-8 Phe207, Leu210, and Leu213 are in van der Waals contacts with hydrophobic residues of GLD-2 helix α_4 . On the other side of the helix, RNP-8 Asp208 and Arg215 form salt bridges with residues on GLD-2 helix α_2 . RNP-8_{GB} ends with a short extended segment interacting with the helical domain (patch 3). Here,

TABLE 1 Data collection and refinement statistics

| GLD-2 _{PAP-D} –RNP-8 _{GB} | |
|---|---|
| Data collection/processing | |
| PDB ID | 5JNB |
| Beamline | X10SA |
| Wavelength (Å) | 0.999 |
| Detector distance (mm) | 395.0 |
| Number of images | 2500 |
| Oscillation range (°) | 0.2 |
| Space group | P1 |
| Cell dimensions | |
| a, b, c (Å) | 65.35, 86.43, 91.91 |
| α , β , γ (°) | 89.88, 93.12, 90.22 |
| Resolution ^a (Å) | 50–2.49 |
| R _{sym} ^a (%) | 8.8 (57.3) |
| I/σ^a | 8.8 (1.8) |
| Completeness ^a (%) | 95.6 (94.6) |
| Redundancy ^a | 2.47 (2.49) |
| Refinement | |
| Resolution (Å) | 46.26–2.49 |
| No. reflections | 135097 |
| R _{work} /R _{free} (%) | 19.19/24.22 |
| Unit cell content | |
| Protein | |
| Chain A | 544–814, 861–878, 883–922 |
| Chain B | 544–815, 861–878, 883–921 |
| Chain C | 544–709, 717–814, 868–765, 774–877, 896–918 |
| Chain D | 549–706, 718–766, 780–813, 871–878, 892–904 |
| Chain E | 177–222 |
| Chain F | 177–222 |
| Chain G | 193–220 |
| Chain H | 195–219 |
| Ions | |
| Sulfate | 4 |
| Magnesium | 2 |
| Water | |
| Ethylene glycol | 9 |
| Average B, all atoms (Å ²) | 53.0 |
| R.m.s. deviations | |
| Bond lengths (Å) | 0.009 |
| Bond angles (°) | 1.194 |
| Ramachandran plot | |
| Allowed (%) | 95.6 |
| Additionally allowed (%) | 3.7 |
| Disallowed (%) | 0.7 |

^aValues in parentheses are for highest resolution shell.

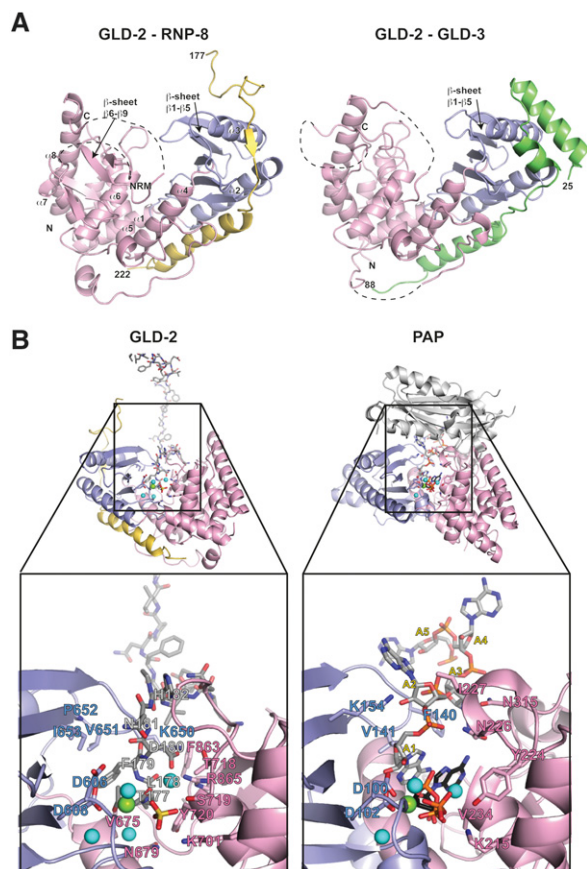


FIGURE 2. Structure of a GLD-2–RNP-8 core complex. (A) Ribbon diagram of the GLD-2_{PAP-D}–RNP-8_{GB} complex (PDB code 5JNB, left panel) and GLD-2_{PAP-D}–GLD-3_{NT} (PDB code 4ZRL, right panel) shown in the same orientation after optimal superposition of their central domains (in pink). The catalytic domains are in blue, RNP-8 in yellow, and GLD-3 in green. The N- and C-terminal residues of the proteins are labeled. Disordered loops are indicated with dashed lines. The five-stranded β -sheet (β 1– β 5) of the catalytic domain is indicated in both structures. In GLD-2_{PAP-D}–RNP-8_{GB}, an additional four-stranded β -sheet (β 6– β 9) is well ordered on top of the central domain. These secondary structure elements correspond to a conserved polypeptide segment between helices α 7 and α 8 and lay on top of helix α 6. NRM, nucleotide recognition motif. (B) On the left is a zoom-in of the active site cleft of the GLD-2_{PAP-D}–RNP-8_{GB} complex shown after a 180° rotation around a vertical axis with respect to the view in panel A. The colors are the same as in panel A, with the peptide of a symmetry-related RNP-8 molecule (for explanations see main text) in stick representation and with carbon atoms in gray. On the right is the corresponding zoom-in view from the structure of canonical PAP bound to RNA and ATP (in stick representation, with carbon atoms in gray and black, respectively) (PDB code 2Q66, Balbo and Bohm 2007). For clarity, the zoom-in view lacks the RRM domain of canonical PAP (shown as a reference in the overall view in light gray). Magnesium and water molecules are shown as green and cyan spheres, respectively. A set of important residues in both GLD-2–RNP-8_{GB} and PAP are highlighted in stick representation and labeled. Note that the place of the two most 3' end ribonucleotides is taken by RNP-8 Phe179 and His182 (instead of the nucleotide bases) and Asn181 (instead of the nucleotide ribose moieties). The place of ATP is taken by RNP-8 Thr177, Leu178, and Asp180 (instead of the adenosine) and by Asp180 and a sulfate ion from the crystallization buffer (instead of the phosphates). Remarkably, the GLD-2_{PAP-D}–RNP-8_{GB} structure also shows a similar arrangement of magnesium and water molecules in the active site as observed in the PAP–RNA–ATP structure (Balbo and Bohm 2007).

two proline residues (RNP-8 219 and 222) pack against two tryptophan residues of GLD-2 (Fig. 3B, right panel).

RNP-8_{GB} and GLD-3_{NT} bind with the same direction and on the same surfaces of GLD-2 (Figs. 2A, 3A–C). This is remarkable because they share little similarity in secondary structure elements. Structural comparisons show that the only portion of RNP-8_{GB} and GLD-3_{NT} that can be superimposed is a four-residue segment (centered at RNP-8_{GB} Tyr200) that binds between patch 1 and patch 2 (Fig. 3D). While both proteins form a helix upon binding to patch 2, their position and interacting residues differ (Fig. 3B,C, middle panels). Conversely, the RNP-8_{GB} and GLD-3_{NT} segments that bind to patch 1 and patch 3 have different structures but position side chains with similar chemical properties to interact with the same residues of GLD-2 (Fig. 3B,C, left and right panels). Consistent with the structural analysis, the Arg574Glu GLD-2 mutant loses the capacity of interacting with either GLD-3_{NT} (Nakel et al. 2015) or RNP-8_{GB} (Fig. 3E), whereas the Asn629Ala mutation has no influence on the binding of the co-factors (Fig. 3E; Nakel et al. 2015). Finally, most of the *C. elegans* GLD-2 residues that interact with both RNP-8 and GLD-3 are evolutionarily conserved or share similar chemical properties (Supplemental Fig. 2), raising the possibility that GLD-2 orthologs might use the same surfaces to bind other proteins. Indeed, bioinformatics analyses suggest the presence of similar hydrophobic hotspots in the GLD-2–binding region of Musashi, a GLD-2 binding partner in *Xenopus* oocytes (Supplemental Fig. 2B; Cragle and MacNicol 2014). The structural information we obtained on the *C. elegans* GLD-2 complexes may thus be useful in the future to identify and characterize other GLD-2 binding proteins in different model organisms.

The finding that RNP-8 and GLD-3 use different amino-acid sequences to compete for the same residues of GLD-2 rationalizes how they can form mutually exclusive poly(A)-polymerase complexes even if they share no apparent conservation at the sequence level. With respect to the observed genetic antagonism between GLD-3 and RNP-8 in early gametogenesis to promote opposite gamete sex (Kim et al. 2009), we presume that at the molecular level selective complex formation may be strongly influenced through developmentally induced changes in protein stoichiometry. Consistent with an abundant protein expression of all three proteins in mid-oogenesis (Eckmann et al. 2002; Wang et al. 2002; Kim et al. 2009), both complexes coexist to synergize in promoting the final stages of oogenesis (Kim et al. 2009, 2010). While a dynamic exchange between both GLD-2-interacting proteins is possible and likely, RNP-8 expression is lost during oocyte activation (Kim et al. 2010), leaving freed GLD-2 to form either further complexes with GLD-3 isoforms or other, hitherto undiscovered maternal proteins to regulate embryonic mRNA fates. In either case, RNP-8 and GLD-3 belong to distinct protein families and their additional potential interaction space is likely to funnel GLD-2_{PAP} activity to select RNA targets.

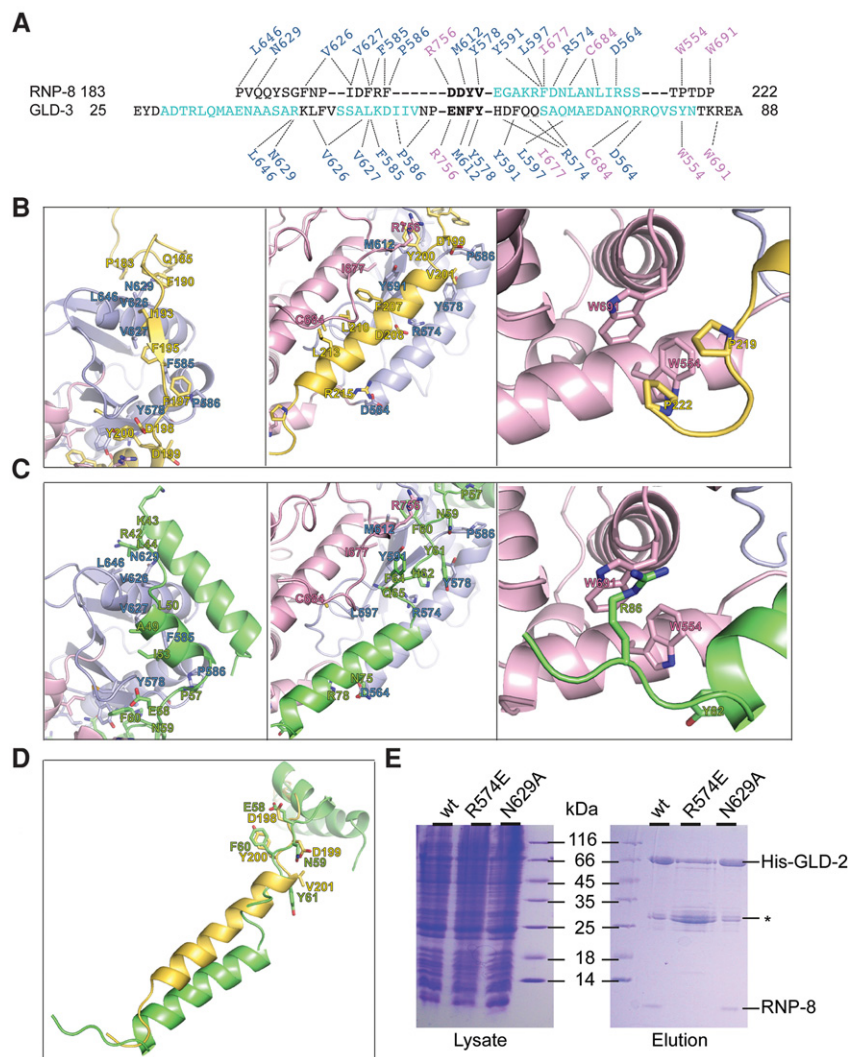


FIGURE 3. Structural basis of mutually exclusive GLD-2–RNP-8 and GLD-2–GLD-3 complex formation. (A) Structural alignment from *C. elegans* RNP-8_{GB} and GLD-3_{NT} with α -helical residues in cyan. Note that only the DDYV segment of RNP-8 and the ENFY segment of GLD-3 (both shown in bold letters) superpose well, with a C- α root mean square deviation of <0.1 Å. The dotted lines indicate the interactions of different GLD-3 and RNP-8 residues with the same side chains in the GLD-2 catalytic and central domains (in blue and pink above and below the sequences). (B) Zoom-in of RNP-8_{GB} interactions with patch 1, patch 2, and patch 3 surfaces of GLD-2 (right, middle, and left panels, respectively). In the middle panel, note that the RNP-8_{GB} helix is close to helix $\alpha 4$ of the GLD-2 central domain and that the GLD-2 loop containing Arg756 binds on top of the RNP-8_{GB} helix. (C) Corresponding zoom-in of GLD-3_{NT} interactions with the same surface patches of GLD-2 (PDB code 4ZRL, Nakel et al. 2015). In the left panel, two GLD-3 residues previously shown to contribute to RNA binding are indicated (Arg42, Lys43, Nakel et al. 2015). In the middle panel, note that the GLD-3_{NT} C-terminal helix is further apart from helix $\alpha 4$ of the GLD-2 central domain and that the GLD-2 loop containing Arg756 binds in between. (D) Superposition of RNP-8 and GLD-3 from the corresponding GLD-2-bound structures. The residues in the DDYV and ENFY segments are indicated. (E) Coomassie-stained 17% SDS/PAGE of His-pull-down experiments of coexpressed wild-type (wt) and mutant His-GLD-2_{PAP} with RNP-8_{GB}. Total lysate control is shown on the left; pulled-down protein eluate is shown on the right. The experiment includes the disrupting GLD-2 R574E mutant (which targets a central residue at the interaction interface) and as a control the GLD-2 N629A mutant (that still supports RNP-8 binding). (*) GST-6xHis-Tag contamination.

In summary, both RNP-8_{GB} and GLD-3_{NT} activate GLD-2_{PAP} with an indirect mechanism, as they both exert a stabilizing effect by covering unfavorable hydrophobic patches

exposed on the surface of the poly(A)-polymerase. Only GLD-3_{NT}, however, appears to stimulate GLD-2 activity directly by contributing RNA-binding residues (Nakel et al. 2015). RNP-8_{GB} lacks analogous residues and indeed has a weaker effect on GLD-2 activation in vitro. Finally, both GLD-2 complexes have a preference for RNA substrates with at least an adenosine at the 3' end. The 3' end substrate preference is thus a general attribute of GLD-2 that is independent of its binding partners.

MATERIALS AND METHODS

Protein expression and purification

The expression vector for the poly(A)-polymerase region of *C. elegans* GLD-2 was previously described (Nakel et al. 2015). It contains the GLD-2 catalytic and central domains (residues 528–923) and lacks a large flexible loop (residues 815–856), and also includes an N-terminal His-tag cleavable by tobacco etch virus (TEV) protease (pETM30 vector). The synthetic gene for *C. elegans* RNP-8 residues 171–250 was obtained from AdB Serotec/Slonomics and was subcloned in an expression vector without tag (pET21 vector). The GLD-2 and RNP-8 vectors were coexpressed in *E. coli* BL21 Gold pLyS cells (Stratagene) using Terrific Broth (TB) medium and overnight induction at 18°C. All proteins were purified with a similar protocol. Cells were lysed in a buffer containing 500 mM NaCl and protease inhibitors (Roche) and the lysate was loaded on a Ni-NTA affinity column (His60, GE Healthcare). After elution and tag cleavage, the complex was further purified by ion exchange chromatography (Q Sepharose, GE Healthcare) and size exclusion chromatography (Superdex, GE Healthcare). The complex was concentrated to 10 mg/mL in 20 mM Tris pH 7.5, 150 mM NaCl, and 4 mM DTT. GLD-2_{PAP} mutants and GLD-3_{NT} were purified as previously described (Nakel et al. 2015).

Crystallization and structure determination

In the initial crystallization trials, GLD-2_{PAP-D}–RNP-8_{GB} (10 mg/mL) were mixed with an 8mer poly(A) RNA substrate, ATP and MgSO₄ in a 1:1,2, 1:2, and 1:4 molar ratio, respectively. Crystals of GLD-2_{PAP-D}–RNP-8_{GB} grew at 20°C in a sitting-drop vapor diffusion setup using as reservoir solution 18% (v/v) polyethyleneglycol

monomethylether (PEG MME) 550, 50 mM potassium nitrate, 60 mM magnesium nitrate, and 30 mM Hepes pH 7.0. Single crystals appeared in a few days. They were transferred to a cryo-protectant solution containing 15% (v/v) ethylene glycol and flash-cooled in liquid nitrogen. Native data were collected on the beamline PXII at the Swiss Light Source (Switzerland) at 100K and processed with XDS (Kabsch 2010). The crystals belong to a triclinic space-group with four molecules in the asymmetric unit. The initial phases were obtained by molecular replacement using Phaser (PHENIX) with the GLD-2_{PAP} structure (PDB ID 4ZRL) as search model (McCoy et al. 2007; Adams et al. 2010). Manual model building and iterative refinement cycles were performed using COOT (Emsley and Cowtan 2004; Emsley et al. 2010), and PHENIX (Adams et al. 2010). No RNA could be detected in the electron density. Detailed data collection and refinement statistics are summarized in Table 1.

Biochemical and biophysical assays

Coexpressions were performed with wild-type and mutant His-GLD-2_{PAP} and RNP-8_{GB} in 200 mL TB overnight at 18°C. For pull-down assays, cells were lysed in 10 mL of 50 mM Tris pH 7.5, 500 mM NaCl, 20 mM Imidazole, and 5 mM β-Mercaptoethanol. The lysates were loaded on 700 μL of Ni-NTA resin at 4°C and the resin was washed with 10 column volumes of lysis buffer. The proteins were eluted in 2 mL of 20 mM Tris pH 7.5, 50 mM NaCl, 250 mM Imidazole, and 5 mM β-Mercaptoethanol.

Polyadenylation assays were performed in a 10-μL reaction volume containing 25 mM Tris pH 8.0, 20 mM KCl, 5 mM MgCl₂, 10% (vol/vol) glycerol, 0.02% (vol/vol) Nonidet P-40, 1 mM DTT, and 0.05 mg/mL BSA. Final concentrations were either 20, 100, or 500 nM for proteins and 0.5 mM for ATP. The appropriate 5'-³²P-labeled RNA synthetic oligos (from biomers.net) were added to a final concentration of 100 nM to start the reaction. Reaction mixtures were incubated at 30°C for 10 min and quenched by adding 10 μL of a buffer containing 50 mM EDTA, 0.1% SDS, and 2 mg/mL Proteinase K (New England Biolabs). Samples were incubated for 10 min at 37°C before diluting 1:3 in 95% (vol/vol) formamide, 10 mM EDTA, 0.1% bromophenol blue, 0.1% xylene cyanole, and loading 2 μL of each reaction on a 10% (wt/vol) polyacrylamide/7M urea gel. Gels were exposed overnight at -80°C to Fuji image plates and visualized using a Typhoon FLA 7000 phosphorimager (GE Healthcare).

For Thermofluor measurements, solutions containing 5 μL of protein (2 mg/mL) and 45 μL of buffer (20 mM Tris pH 7.5, 150 mM NaCl, and 10% Glycerol) with 3.9X of Sypro Orange (Invitrogen) were added to the wells of a 96-well Twin-tec plate (Eppendorf). The plate was sealed and heated in a real-time PCR system (Eppendorf) from 20°C to 80°C in increments of 0.5°C. Fluorescence changes were monitored simultaneously. The wavelengths for excitation and emission were 470 and 550 nm, respectively. A Boltzmann model was used to fit the fluorescence data after normalization and obtain the temperature midpoint for the protein unfolding transition (T_m).

SUPPLEMENTAL MATERIAL

Supplemental material is available for this article.

DATA DEPOSITION

The coordinates and the structure factors have been deposited in the Protein Data Bank with the accession code 5JNB.

ACKNOWLEDGMENTS

We thank the staff of the MPIB Crystallization and Core facility and of the PX beamlines at the Swiss Light Source (Villigen, Switzerland). This study was supported by the Max Planck Gesellschaft, the European Commission (ERC Advanced Investigator Grant 294371 and Marie Curie ITN RNPnet) and the Deutsche Forschungsgemeinschaft (DFG SFB646, SFB1035, GRK1721, FOR1680, and CIPSM) to E.C., DFG EC369/3-1, GRK1591 to C.R.E., and BU2451/1-2 to K.N.

Author contributions: K.N. solved the structure; F.B. performed the biochemical assays; C.B. did the thermofluor assay and B.H. the Musashi alignment; E.C. and C.R.E. initiated the project; E.C. and K.N. wrote the manuscript.

Received March 21, 2016; accepted April 28, 2016.

REFERENCES

- Adams PD, Afonine PV, Bunkoczi G, Chen VB, Davis IW, Echols N, Headd JJ, Hung LW, Kapral GJ, Grosse-Kunstleve RW, et al. 2010. PHENIX: a comprehensive Python-based system for macromolecular structure solution. *Acta Crystallogr D Biol Crystallogr* **66**: 213–221.
- Balbo PB, Bohm A. 2007. Mechanism of poly(A) polymerase: structure of the enzyme-MgATP-RNA ternary complex and kinetic analysis. *Structure* **15**: 1117–1131.
- Barnard DC, Ryan K, Manley JL, Richter JD. 2004. Symplekin and xGLD-2 are required for CPEB-mediated cytoplasmic polyadenylation. *Cell* **119**: 641–651.
- Benoit P, Papin C, Kwak JE, Wickens M, Simonelig M. 2008. PAP- and GLD-2-type poly(A) polymerases are required sequentially in cytoplasmic polyadenylation and oogenesis in *Drosophila*. *Development* **135**: 1969–1979.
- Cragle C, MacNicol AM. 2014. Musashi protein-directed translational activation of target mRNAs is mediated by the poly(A) polymerase, germ line development defective-2. *J Biol Chem* **289**: 14239–14251.
- Crittenden SL, Eckmann CR, Wang L, Bernstein DS, Wickens M, Kimble J. 2003. Regulation of the mitosis/meiosis decision in the *Caenorhabditis elegans* germline. *Philos Trans R Soc Lond B Biol Sci* **358**: 1359–1362.
- Cui J, Sartain CV, Pleiss JA, Wolfner MF. 2013. Cytoplasmic polyadenylation is a major mRNA regulator during oogenesis and egg activation in *Drosophila*. *Dev Biol* **383**: 121–131.
- Eckmann CR, Kraemer B, Wickens M, Kimble J. 2002. GLD-3, a bicaudal-C homolog that inhibits FBF to control germline sex determination in *C. elegans*. *Dev Cell* **3**: 697–710.
- Eckmann CR, Crittenden SL, Suh N, Kimble J. 2004. GLD-3 and control of the mitosis/meiosis decision in the germline of *Caenorhabditis elegans*. *Genetics* **168**: 147–160.
- Eckmann CR, Rammelt C, Wahle E. 2011. Control of poly(A) tail length. *Wiley Interdiscip Rev RNA* **2**: 348–361.
- Emsley P, Cowtan K. 2004. Coot: model-building tools for molecular graphics. *Acta Crystallogr D Biol Crystallogr* **60**: 2126–2132.
- Emsley P, Lohkamp B, Scott WG, Cowtan K. 2010. Features and development of Coot. *Acta Crystallogr D Biol Crystallogr* **66**: 486–501.
- Hansen D, Hubbard EJA, Schedl T. 2004. Multi-pathway control of the proliferation versus meiotic development decision in the *Caenorhabditis elegans* germline. *Dev Biol* **268**: 342–357.
- Kabsch W. 2010. Xds. *Acta Crystallogr D Biol Crystallogr* **66**: 125–132.

- Kadyk LC, Kimble J. 1998. Genetic regulation of entry into meiosis in *Caenorhabditis elegans*. *Development* **125**: 1803–1813.
- Kim KW, Nykamp K, Suh N, Bachorik JL, Wang L, Kimble J. 2009. Antagonism between GLD-2 binding partners controls gamete sex. *Dev Cell* **16**: 723–733.
- Kim KW, Wilson TL, Kimble J. 2010. GLD-2/RNP-8 cytoplasmic poly(A) polymerase is a broad-spectrum regulator of the oogenesis program. *Proc Natl Acad Sci* **107**: 17445–17450.
- Krissinel E, Henrick K. 2007. Inference of macromolecular assemblies from crystalline state. *J Mol Biol* **372**: 774–797.
- Kwak JE, Wang L, Ballantyne S, Kimble J, Wickens M. 2004. Mammalian GLD-2 homologs are poly(A) polymerases. *Proc Natl Acad Sci* **101**: 4407–4412.
- Kwak JE, Drier E, Barbee SA, Ramaswami M, Yin JC, Wickens M. 2008. GLD2 poly(A) polymerase is required for long-term memory. *Proc Natl Acad Sci* **105**: 14644–14649.
- Martin G, Keller W. 2007. RNA-specific ribonucleotidyl transferases. *RNA* **13**: 1834–1849.
- McCoy AJ, Grosse-Kunstleve RW, Adams PD, Winn MD, Storoni LC, Read RJ. 2007. Phaser crystallographic software. *J Appl Crystallogr* **40**: 658–674.
- Moore MJ, Proudfoot NJ. 2009. Pre-mRNA processing reaches back to transcription and ahead to translation. *Cell* **136**: 688–700.
- Nakel K, Hartung SA, Bonneau F, Eckmann CR, Conti E. 2010. Four KH domains of the *C. elegans* Bicaudal-C ortholog GLD-3 form a globular structural platform. *RNA* **16**: 2058–2067.
- Nakel K, Bonneau F, Eckmann CR, Conti E. 2015. Structural basis for the activation of the *C. elegans* noncanonical cytoplasmic poly(A)-polymerase GLD-2 by GLD-3. *Proc Natl Acad Sci* **112**: 8614–8619.
- Norbury CJ. 2013. Cytoplasmic RNA: a case of the tail wagging the dog. *Nat Rev Mol Cell Biol* **14**: 643–653.
- Nousch M, Yeroslaviz A, Habermann B, Eckmann CR. 2014. The cytoplasmic poly(A) polymerases GLD-2 and GLD-4 promote general gene expression via distinct mechanisms. *Nucleic Acids Res* **42**: 11622–11633.
- Papin C, Rouget C, Mandart E. 2008. *Xenopus* Rbm9 is a novel interactor of XGld2 in the cytoplasmic polyadenylation complex. *FEBS J* **275**: 490–503.
- Rouhana L, Wickens M. 2007. Autoregulation of GLD-2 cytoplasmic poly(A) polymerase. *RNA* **13**: 188–199.
- Sartain CV, Cui J, Meisel RP, Wolfner MF. 2011. The poly(A) polymerase GLD2 is required for spermatogenesis in *Drosophila melanogaster*. *Development* **138**: 1619–1629.
- Schmidt MJ, Norbury CJ. 2010. Polyadenylation and beyond: emerging roles for noncanonical poly(A) polymerases. *Wiley Interdiscip Rev RNA* **1**: 142–151.
- Suh N, Jedamzik B, Eckmann CR, Wickens M, Kimble J. 2006. The GLD-2 poly(A) polymerase activates *gld-1* mRNA in the *Caenorhabditis elegans* germ line. *Proc Natl Acad Sci* **103**: 15108–15112.
- Udagawa T, Swanger SA, Takeuchi K, Kim JH, Nalavadi V, Shin J, Lorenz LJ, Zukin RS, Bassell GJ, Richter JD. 2012. Bidirectional control of mRNA translation and synaptic plasticity by the cytoplasmic polyadenylation complex. *Mol Cell* **47**: 253–266.
- Wang L, Eckmann CR, Kadyk LC, Wickens M, Kimble J. 2002. A regulatory cytoplasmic poly(A) polymerase in *Caenorhabditis elegans*. *Nature* **419**: 312–316.
- Weill L, Belloc E, Bava FA, Méndez R. 2012. Translational control by changes in poly(A) tail length: recycling mRNAs. *Nat Struct Mol Biol* **19**: 577–585.



RNA

A PUBLICATION OF THE RNA SOCIETY

Structural basis for the antagonistic roles of RNP-8 and GLD-3 in GLD-2 poly(A)-polymerase activity

Katharina Nakel, Fabien Bonneau, Claire Basquin, et al.

RNA 2016 22: 1139-1145 originally published online June 10, 2016
Access the most recent version at doi:[10.1261/rna.056598.116](https://doi.org/10.1261/rna.056598.116)

Supplemental Material <http://rnajournal.cshlp.org/content/suppl/2016/06/10/rna.056598.116.DC1.html>

References This article cites 35 articles, 15 of which can be accessed free at:
<http://rnajournal.cshlp.org/content/22/8/1139.full.html#ref-list-1>

Open Access Freely available online through the *RNA* Open Access option.

Creative Commons License This article, published in *RNA*, is available under a Creative Commons License (Attribution 4.0 International), as described at <http://creativecommons.org/licenses/by/4.0/>.

Email Alerting Service Receive free email alerts when new articles cite this article - sign up in the box at the top right corner of the article or [click here](#).



Webinar: Successful microRNA qPCR
in challenging samples

EXIQON

To subscribe to *RNA* go to:
<http://rnajournal.cshlp.org/subscriptions>
